Progress in Physics of Applied Materials 2 (2022) 147–156

Semnan University

Progress in Physics of Applied Materials

journal homepage: https://ppam.semnan.ac.ir/

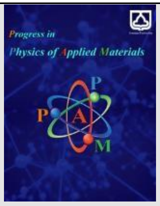

Structural and physical properties of Co$_{1-x}$Cd$_x$Fe$_2$O$_4$ /SiO$_2$ nanocomposites

R. Ghasemi[1], M. Naseri[1*], D. Souri[1], A. Kamalianfar[2]

[1]*Department of Physics, Malayer University, Malayer, Iran*
[2]*Department of Physics, Farhangian University, Tehran 1998963341, Iran*

ARTICLE INFO

Article history:
Received: 10 November 2022
Revised: 24 December 2022
Accepted: 24 December 2022

Keywords:
Nanocomposites
Magnetic properties
Ferrites
SiO$_2$

ABSTRACT

The preparation of Co$_{1-x}$Cd$_x$Fe$_2$O$_4$/SiO$_2$ nanocomposites with core/ shell structure involved the coating of SiO$_2$ using Stöber method on Co$_{1-x}$Cd$_x$Fe$_2$O$_4$ and the use of facile thermal treatment method for synthesizing nanoparticles. The effect of cadmium substitution and SiO$_2$ coating on the degree of crystallinity, samples composition, microstructure, and phase composition were conducted by X-ray diffraction (XRD), energy dispersion X-ray analysis (EDXA), transmission electron microscopy (TEM), and fourier transform infrared spectroscopy (FT-IR), respectively. Magnetic properties were demonstrated by a vibrating sample magnetometer (VSM) which displayed that Co-Cd ferrite nanoparticles and coated silica samples exhibited magnetic behaviors. In investigating the influence of cadmium substitution and the SiO$_2$ coating on the band gap energy (E$_g$), a more accurate method was used in evaluating the band gap energy (Eg). The method of evaluation is a recently proposed one known as derivation of absorption spectrum fitting (DASF) which involves the direct absorption spectra of UV-Visible region, without any need for the concentration of powders or solutions.

1. Introduction

In recent times, magnetic nanoparticles have considerably been applied in different fields such as magnetic, electronic, and catalytic applications like biomedical drug technology, high density magnetic recording, magnetic resonance imaging, ferrofluid technology, waste water treatment, data storage, biosensors, and biocompatible magnetic nanoparticles for cancer treatment and magneto-optical devices [1-2].

Spinel ferrites is one of the commonly known magnetic materials with the general formula of $A^{2+} B_2^{3+} O_4$ whereby, A (the tetrahedral site) represents a divalent metal ion and B (the octahedral site) represents a trivalent metal ion [3]. One of the most relevant ferrite is a reverse CoFe$_2$O$_4$ spinel structure, where a fcc lattice is made up of oxygen atoms and one half of Fe^{3+} ions occupies the tetrahedral A sites and the other half, together with Co^{2+} ions occupy the octahedral B sites [4]. A typical spinel ferrite which can be used in various fields is cadmium ferrite (CdFe$_2$O$_4$) nanoparticles. In bulk form, cadmium ferrite has a normal spinel structure in which all Cd^{2+} ions are in A sites and Fe^{3+} ions are distributed in B sites [5]. Different composition of cations can appropriately tailor the magnetic properties of ferrites. When ferrite is doped with small amount of nonmagnetic ions such as Zn^{2+} or Cd^{2+}, the saturation of magnetization is augmented [4, 6].

Due to the emergence of core/shell nanocomposites in the field of materials chemistry and other fields like biomedical, catalysis, electronics, optics, and pharmaceutical, it is gradually gaining more attention in the research and practice continuum. Coating of the core particle enables the modification of the surface, stability, ability to increase functionality, dispersibility, regulated release of the core, and less consumption of precious materials [7].

Through investigations that have been conducted in recent times, it has been found that silica is more appropriate for coating due to the fact that there is strong bond between the surface of magnetite and silica. When silica is used for coating, primer is not required for the advancement of its deposition and adhesion. In addition, silica has high chemical and thermal stabilities, non-toxicity properties and is highly compatible with other materials. The silica/magnetic core–shell structured nanoparticle composites which provide wide surface areas for binding different biological ligands or other materials on their surface, also has the ability to be uniformly distributed in aqueous solutions without the addition of other surfactants in a wide range of pH values [8, 9].

Thus, the focus of the current study is the use of Cd^{2+} ions to substitute cobalt ferrite nanoparticles in order to

---

* Corresponding author. Tel.: +98-9126868423
E-mail address: m.naseri@malayeru.ac.ir

DOI: **10.22075/ppam.2022.28952.1039**

examine its effect on magnetic, structural, and optical properties through the use of thermal treatment method which is a convenient and simple environmentally friendly method. This method is also convenient in the sense that it is less expensive, does not utilize or produce toxic substances, and has low reaction temperatures which makes it appropriate for use in industrial applications [10]. Moreover, a special emphasis is given to the Stöber method, which is relatively simple, effective, and well verified for the synthesis of large and highly uniform silica particles [11].

2. Experimental

2.1 Materials

Poly Vinyl Pyrrolidon (PVP), Iron nitrate $Fe(NO_3)_3.9H_2O$, Cobalt nitrate, $Co(NO_3)_2{\cdot}6H_2O$, Cadmium nitrate, $Cd(NO_3)_2.6H_2O$, ethanol, tetraethyl orthosilicate (TEOS), and ammonia aqueous (25 wt%) which were used in the experiments are all analytical grade. Distilled water was used throughout the experiments.

2.2 Synthesis of $Co_{1-x}Cd_xFe_2O_4$ nanoparticles

Magnetic nanoparticles were prepared using a simple thermal treatment. Typically, 3g of PVP were dissolved in 100 ml of distilled water at 343 K, and the obtained transparent solution was mixed with 0.2 mmol of iron nitrate and 0.1 mmol of cobalt nitrate and cadmium nitrate (Fe : Co, Cd=2:1). After constant stirring of 2 h using a magnetic stirrer, the resultant homogeneous solution was poured into a glass Petri dish and heated at 363 K in an oven for 20 h in order to allow the evaporation of water. Afterwards, the obtained dried solid was ground for 20 min in a mortar to form powder. The powder was then annealed for 9 h at 923 K in order to obtain Co-Cd ferrite nanoparticles.

2.3 Synthesis of $Co_{1-x}Cd_xFe_2O_4/SiO_2$ nanocomposites

Following the Stöber method with some modifications, coating of Co-Cd ferrite nanocomposites with a silica layer was carried out in a basic ethanol/water mixture at 30 °C. The nanocomposites were first treated by using distilled water (2 ml), ethanol (6ml), and aqueous ammonia (0.18 ml, 25 wt%). The resultant solution was then homogenized by ultrasonic vibration in water bath. After that, under continuous stirring, 0.22g of TEOS diluted in ethanol (1 ml) was drop-wise added to this dispersion. After stirring for 12 h at room temperature, $Co_{1-x}Cd_xFe_2O_4/SiO_2$ nanocomposites were separated by a permanent magnet and washed with ethanol several times. Finally, the samples were dried at 50 °C for 24 h.

3. Characterization

The $Co_{1-x}Cd_xFe_2O_4$ nanoparticles and $Co_{1-x}Cd_xFe_2O_4/SiO_2$ nanocomposite were characterized through the use of the XRD technique using a PANalytical Company X'Pert PRO MPD type of instrument with Cu Kα radiation and a wave length λ=1.5405 Å radiation so as to generate diffraction patterns from powder crystalline samples at ambient temperature in a 2θ range of 10°–80°.

FT-IR spectra were recorded using a PerkinElmer FTIR model 1650 spectrometer. Prior to recording the spectra, the samples were placed on a Universal ATR Sampling Accessory (diamond coated with CsI) and pressed. The compositions of the samples were determined by energy dispersion X-ray analysis (EDXA), TESCAN Company. The microstructure and particle size of the $Co_{0.2}Cd_{0.8}Fe_2O_4$ nanoparticles and $Co_{0.2}Cd_{0.8}Fe_2O_4/SiO_2$ nanocomposite were determined based on Transmission Electron Microscopy (TEM) images that were obtained using a Philips CM120 version electron microscope at an accelerating voltage of 120 kV. Magnetization measurements were conducted using a VSM (MDKB model) at room temperature with a maximum magnetic field of 10kOe. The band gap energies of the $Co_{1-x}Cd_xFe_2O_4$ nanoparticles and $Co_{1-x}Cd_xFe_2O_4/SiO_2$ nanocomposite were characterized using UV-visible absorption spectroscopy (Perkin Elmer Lambda 25).

4. Results and discussion

4.1. Crystallinity, elemental composition and microstructure of the $Co_{1-x}Cd_xFe_2O_4/SiO_2$ nanocomposites

The structure and phase purity of the samples were confirmed by analyzing the diffraction patterns of X-ray powder. Figs. 1a to 1f show the XRD patterns of $Co_{1-x}Cd_xFe_2O_4$ nanoparticles with different values of Cd concentration from (x) = 0 to (x) = 1. Also a broad peak occurred in the precursor (Fig. 1(g)), which does not have sharp diffraction patterns and is still amorphous. It has been confirmed by using XRD reference cards ICCD: 22-1086 for $CoFe_2O_4$ and ICCD: 22-1063 for $CdFe_2O_4$ that all samples have spinel cubic ferrite nanostructure without any other impurity phases and the formation of a series of solutions between $CoFe_2O_4$ and $CdFe_2O_4$. Based on the XRD patterns in Fig.1, it is clear that crystal planes of $Co_{1-x}Cd_xFe_2O_4$ and $CoFe_2O_4$ nanoparticles are the same.

Fig. 2 shows the XRD patterns of $Co_{1-x}Cd_xFe_2O_4$ /SiO_2 nanocomposites with no significant changes observed in the diffraction peaks. In addition, no characteristic peak was observed in SiO_2, which is due to the low content of SiO_2 in the nanocomposites [12].

Average crystallite size (D) of all the samples is calculated using the Debye-Scherrer equation given by equation (1):

$$D = 0.9\lambda/\beta\cos\theta \qquad (1)$$

Where λ (λ =0.154 nm) is the wavelength of the X-ray radiation used and β is the full width at half maximum (FWHM) intensity in radian. The analysis showed that the crystallite sizes are in the range of 13 to 27 nm. The values of lattice parameter evaluated from the XRD spectra are recorded in Table 1. The increase in lattice constant as a function of Cd concentration, may be due to substitution of large Cd^{2+} ions (0.97 Å) by relatively small Co^{2+} (0.74 Å) [13] ions in the system of $Co_{1-x}Cd_xFe_2O_4$.

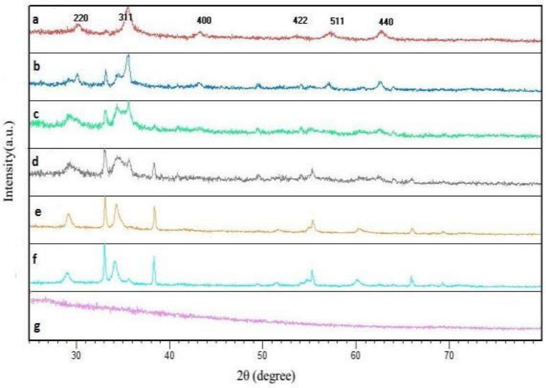

Fig. 1. XRD patterns of $Co_{1-x}Cd_xFe_2O_4$ nanoparticles for (a) x=0, (b) x=0.2, (c) x=0.4, (d) x=0.6, (e) x=0.8, (f) x=1, and (g) precursor.

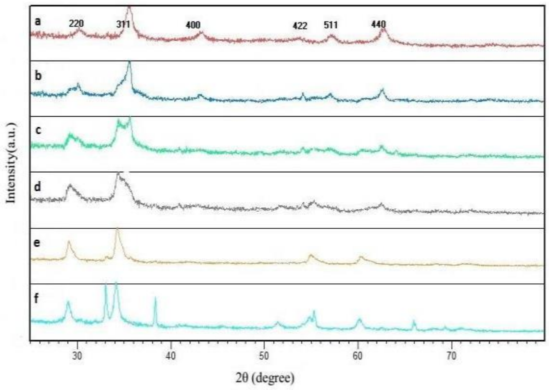

Fig. 2. XRD pattern of $Co_{1-x}Cd_xFe_2O_4/SiO_2$ nanocomposites for (a) x=0, (b) x=0.2, (c) x=0.4, (d) x=0.6, (e) x=0.8, (f) x=1.

Table1: XRD results and Lattice parameter of $Co_{1-x}Cd_xFe_2O_4$ nanoparticles.

Samples	Crystal size (nm)	Lattice parameter (Å)
$CoFe_2O_4$	18	8.3608
$Co_{0.8}Cd_{0.2}Fe_2O_4$	27	8.3540
$Co_{0.6}Cd_{0.4}Fe_2O_4$	27	8.6435
$Co_{0.4}Cd_{0.6}Fe_2O_4$	13	8.6435
$Co_{0.2}Cd_{0.8}Fe_2O_4$	18	8.6753
$CdFe_2O_4$	23	8.6852

Fourier transforms infrared spectrometer (FTIR) was used to verify functional groups of the two samples as shown in Fig. 3. In ferrites nanostructures, it is well known that metal ions are distributed between two lattice sites namely tetrahedral (A) and octahedral (B) with oxygen atoms as their nearest neighbors. Therefore, two main metal-oxygen bands are expected to be present in IR spectra of the uncoated $Co_{0.8}Cd_{0.2}Fe_2O_4$ nanoparticles as shown in Fig. 3a. Moreover, bands appearing from 300 to 1000 cm^{-1} are attributed to the lattice vibrations of metal ions [14]. Higher band (υ_1) was mostly observed in the range 500 to 600 cm^{-1}, which is possibly due to the intrinsic stretching vibrations of metal–oxygen ions (Fe^{3+}-O^{2-}) at tetrahedral sites in spinel structure. On the other hand, the lower band (υ_2) was observed in the range of 385 to 450 cm^{-1} indicating the presence of cation-anions stretching vibrations at octahedral sites Co^{2+}-O^{2-} [4]. The broad absorption region between 3150 and 3450 cm^{-1} and the peak at around 1628 cm^{-1} can be attributed to the stretching vibration of hydrogen-bonded OH groups [15]. An absorption band at around 2350 cm^{-1} is attributed to adsorbed or atmospheric CO_2 [10]. FTIR spectroscopy confirmed the presence of silica network on the surface of the $Co_{0.8}Cd_{0.2}Fe_2O_4$ nanocparticles as depicted in coated $Co_{0.8}Cd_{0.2}Fe_2O_4/SiO_2$ nanocomposites presented in Fig. 3b. These characteristic Si–O–Si peaks were at 1079 and 794 cm^{-1} [16, 17]. The absorptions in the range of 1100 to 1500 cm^{-1} correspond to M-O-M bands (metal-oxygen-metal) such as Co-O-Co and Fe-O-Fe bands [18].

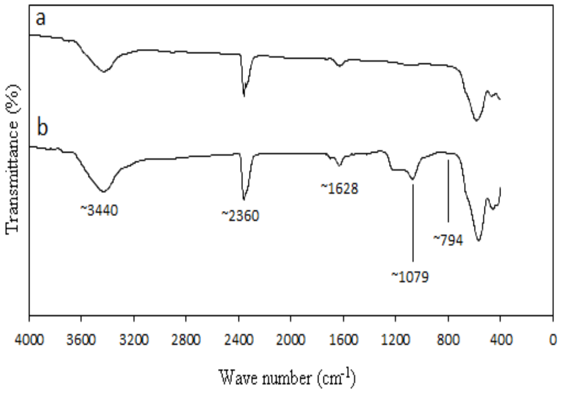

Fig. 3. FITR spectra of (a) uncoated $Co_{0.8}Cd_{0.2}Fe_2O_4$ nanoparticles and (b) coated $Co_{0.8}Cd_{0.2}Fe_2O_4/SiO_2$ nanocomposites.

Fig. 4 presents energy dispersion X-ray analysis of (a) $Co_{0.4}Cd_{0.6}Fe_2O_4$ nanoparticles and (b) $Co_{0.4}Cd_{0.6}Fe_2O_4/SiO_2$ nanocomposites. The elemental analysis in Fig. 4a shows the presence of Co, O, Fe and Cd which confirms the formation of $Co_{0.4}Cd_{0.6}Fe_2O_4$ nanoparticles. Furthermore, the elemental analysis in Fig. 4b indicates the presence of Co, O, Fe, Cd, and Si which also proved the formation of $Co_{0.4}Cd_{0.6}Fe_2O_4/SiO_2$ nanocomposite. The observed results are in accordance with expected amounts of these elements in the nanoparticles. The calculated and measured values of mass percent are tabulated in Table 2. One can see that there is a slight difference between these values, which is an evidence of homogeneous distribution of the elements.

In order to check the morphology and mean crystallite size, nanoparticles were characterized by using TEM images. Fig. 5a shows the bright field TEM micrograph for $Co_{0.2}Cd_{0.8}Fe_2O_4$ nanoparticles. It can be clearly seen that the nanoparticles possess uniform shape and their average particle size was 21 nm. It was also observed that some nanoparticles were agglomerated with each other, and that can be explained by the magneto static interaction between particles. In fact, particles experience a permanent magnetic moment proportional to their volume [18]. Another reason is that several neighboring particles fuse together so as to increase the particle size by the melting of their surfaces [10]. The TEM image of $Co_{0.2}Cd_{0.8}Fe_2O_4/SiO_2$ nanocomposite is shown in Fig. 5b. It can be seen that the $Co_{0.2}Cd_{0.8}Fe_2O_4$ spherical nanoparticles are homogenously distributed within the amorphous silica matrix without any obvious agglomeration.

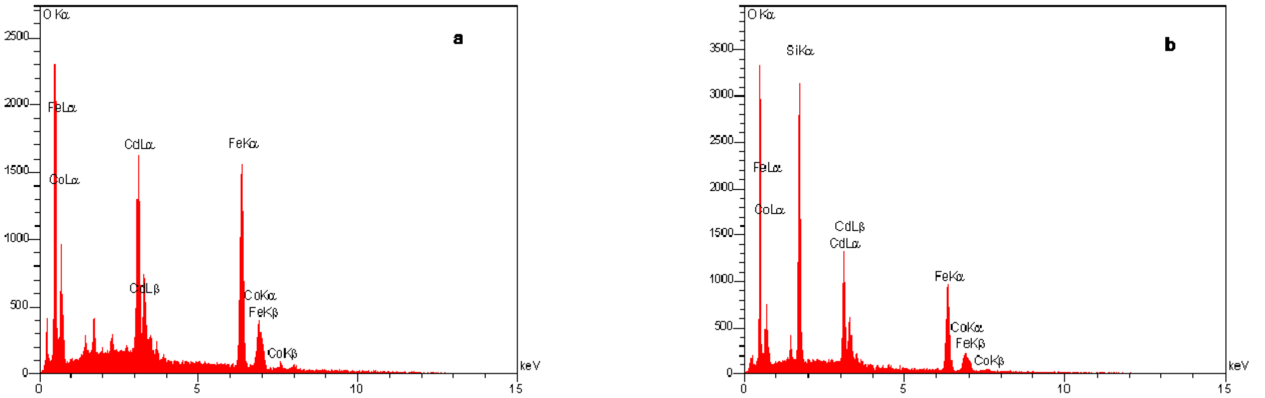

Fig. 4. EDS analysis of (a) $Co_{0.4}Cd_{0.6}Fe_2O_4$ nanoparticles and (b) $Co_{0.4}Cd_{0.6}Fe_2O_4/SiO_2$ nanocomposites.

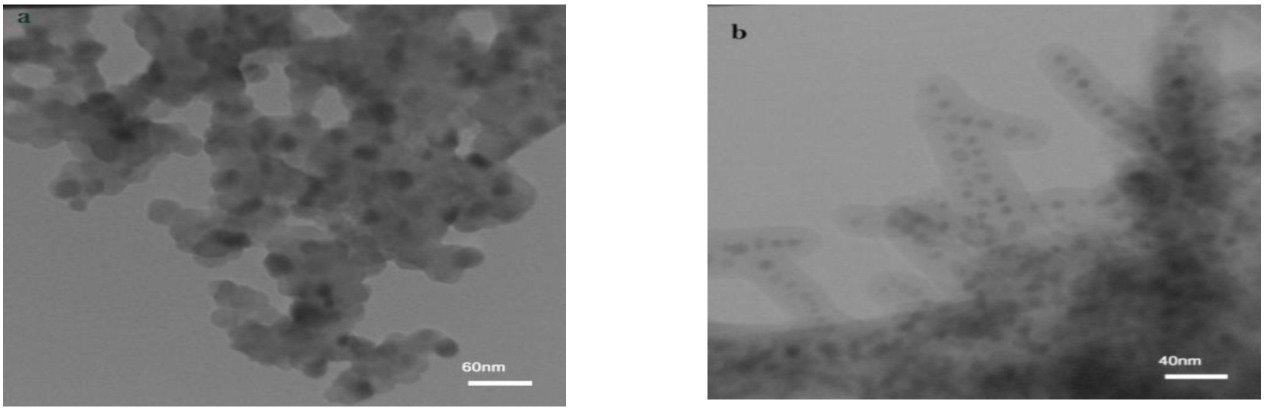

Fig. 5. TEM images for (a) $Co_{0.2}Cd_{0.8}Fe_2O_4$ nanoparticles and (b) $Co_{0.2}Cd_{0.8}Fe_2O_4/SiO_2$ nanocomposites.

Table 2: EDX quantification element of $Co_{0.4}Cd_{0.6}Fe_2O_4$ nanoparticles.

Element	W(%) measured	W(%) calculated
O	28.24	23.98
Fe	35.66	41.88
Co	9.56	8.83
Cd	26.54	25.2
Si	-	-
total	100	100

This is due to the fact that the silica matrix is not only known to serve as spatial nucleation sites for $Co_{0.2}Cd_{0.8}Fe_2O_4$ nanoparticles, but also to confine the coarsening of nanoparticles while minimizing the degree of crystallite aggregation [19]. The mean particle sizes were estimated around 8 nm.

4.2. Magnetics and optical properties of the $Co_{1-x}Cd_xFe_2O_4/SiO_2$ nanocomposites

Typical hysteresis loops of coated and uncoated samples for different concentrations are shown in Figs. 6 and 7. The different values of saturation magnetization (M_s), remanence magnetization (M_r), and coercivity (H_c) of $Co_{1-x}Cd_xFe_2O_4$ nanoparticles as well as $Co_{1-x}Cd_xFe_2O_4/SiO_2$ nanocomposites are listed in Table 3. As seen in Fig. 6, when x increases from 0 to 0.8, M_s, M_r, and H_c decrease from 36 emu/g, 6.48 emu/g, and 498.9 Oe to 2.59 emu/g, 0.14 emu/g, and 39.28 Oe, respectively. It is clear that pure $CoFe_2O_4$ nanoparticles demonstrate ferromagnetic behavior by increasing the concentration of cadmium.

The superparamagnetic effect becomes more intense because of reduction of ferromagnetic behavior, so that, pure $CdFe_2O_4$ nanoparticles are superparamagnetic. It is well known that the magnetic properties of ferrite nanoparticles depend on several parameters such as processing conditions, chemical compositions, and distributions of cations in tetrahedral (A-site) and octahedral (B-site) positions. Therefore, the occupancy of the cations in these sites determine the magnetic behavior of the nanoparticles [20].

Difference in the saturation magnetization values can be attributed to the surface order/disorder interaction of magnetic spin moment and the disturbance in the spinel structure inversion [21]. Also, the changes in magnetization can be due to non-saturation effects of randomly distributed small particles having high magneto-crystalline anisotropy [22]. The distorted cation distribution, canted spin, and presence of a dead layer on the surface of the particles are responsible for decrease in the saturation magnetization [23]. In the case of this study, the decrease in M_s and M_r with Cd content may be explained as follows; Cd^{2+} ions weaken magnetic super-exchange interactions between A and B sites. Cd^{2+} ions have larger ionic radius (0.97 Å) than Co^{2+} (0.74 Å), so the Cd^{2+} substitution distorts the lattice and destroys the homogeneous composition thereby leading to the deterioration in n_B due to antiferromagnetic coupling, and then the net overall magnetic moment ($n_B = M_A - M_B$) decreases [13].

$CoFe_2O_4$ has an inverse spinel structure in the form of $[Co_\delta Fe_{1-\delta}]^A [Co_{1-\delta} Fe_{1+\delta}]^B O_4$, where A and B represents the tetrahedral and octahedral sites respectively and δ is the inversion parameter. In the case of $\delta = 1$, the ferrite has spinel structure like $CdFe_2O_4$ and in the other case, i.e., $\delta=0$, structure becomes inverse spinel and a typical example is $CoFe_2O_4$. Inter-sub-lattice, super-exchange interactions of the cations on the (A-B) are much stronger than the (A-A) and (B-B) intra-sub-lattice exchange interactions [24].

The substitution of Cd^{2+} at B sites for Co^{2+} may reduce the net magnetic moment at B sites as the magnetic moment of Cd^{2+} ($0\mu_B$) is less than that of Co^{2+} ($3\mu_B$). This replacement weakens the A-B super-exchange interactions while B-B interaction becomes prominent. Consequently, parallel arrangement of spin magnetic moments on B-site is disturbed. This behavior can be better understood by Yaffet-Kittel's (Y-K) three-sublattice model which must be used to calculate the magnetic moment of the samples [25]. In this model, the magnetic moment is calculated by equation (2):

$$n_B = M_B \, \text{Cos}_{\alpha YK} - M_A \qquad (2)$$

According to this model, the magnetic moment of the B sites is composed of two components B1 and B2, which have equal value with the Y-K angle (αy-k) between them [25]. This is due to the difference in the value of the theoretical magnetic moment and experimental magnetic moment [26]. Thus in equation 2, when surplus Cd^{2+} ions are substituted, B–B interaction becomes the main exchange and the canted spins decrease the magnetization of the ferrite [24].

Fig. 7 shows the hysteresis loops of $Co_{1-x}Cd_xFe_2O_4/SiO_2$ nanocomposites. It can be seen from Fig. 7 that the saturation magnetization values of the core-shell are lower than those of the uncoated ferrite nanoparticles. The decrease in magnetization values is mainly due to the contribution of the volume of the nonmagnetic coating layer to the total sample value. It is noteworthy that the nonmagnetic layer can be considered as a magnetically dead layer over the surface of nanoparticles, thus affecting the magnitude or uniformity of magnetization owing to quenching of surface moment [27]. Silica shell separates each particle from its neighbors thereby decreasing the magneto static coupling between the particles [28].

The coercivity is defined as a measure of the magnetic strength that is required to achieve changes of magnetization direction in a material. Coercivity in a ferrite system is known to depend on several parameters such as anisotropy constant, lattice imperfections, internal strains, and grain size [29].

The values of H_c in Table 3 show that, decrease in coercivity can be explained by considering direct effect of H_c on anisotropy. A reason for decrease in coercivity is that the anisotropy of spinel ferrites depends on Fe concentration in the samples. By increasing Cd^{2+} in cobalt ferrite magneto crystalline, anisotropy will decrease through the immigration of Co^{2+} ions to tetrahedral site by reducing the concentration of Fe^{2+} ions [4].

One of the most crucial things to remember is that, the decrease in H_c is due to the fact that the higher ferrite content consists of a greater number of domain walls. The magnetization or demagnetization caused by the domain wall movement requires less energy. As the number of walls increase with crystallite size, the contribution of wall movement to magnetization or demagnetization becomes greater than that of single-domain rotation [30].

Therefore, the samples with higher ferrite content are expected to have a lower coercivity. In comparison, the coercivity of the uncoated samples is lesser than those of the silica-coated. This can be attributed to the fact that $Co_{1-x}Cd_xFe_2O_4$ nanoparticles have lower magnetic anisotropy than those samples coated by SiO_2, because of the intrinsic anisotropy of the particles enhanced by the inter-particles dipolar fields of cobalt ferrite in silica matrix [31].

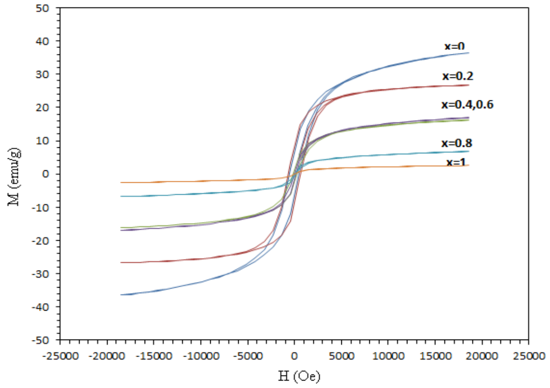

Fig. 6. Magnetic hysteresis loops of $Co_{1-x}Cd_xFe_2O_4$ nanoparticles.

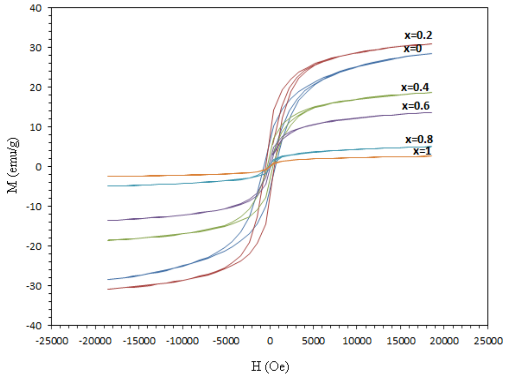

Fig. 7. Magnetic hysteresis loops of $Co_{1-x}Cd_xFe_2O_4/SiO_2$ nanocomposites.

The optical band gap is the most important characteristic of materials that are good choices for optoelectronic applications. Furthermore, precise evaluation of optical band gap is very important, because it can affect the device optimizations. Energy values corresponding to the band gap (E_g) between the valance and the conduction bands can be determined using well known Tauc relation [32] given by equation (3):

$$\alpha E = \alpha_0 (E - E_g)^\delta \qquad (3)$$

Table 3: Magnetic and optical parameters of uncoated $Co_{1-x}Cd_xFe_2O_4$ nanoparticles and coated $Co_{1-x}Cd_xFe_2O_4/SiO_2$ nanocomposites.

Sample	M_s (emu/g)	H_c (Oe)	M_r (emu/g)	Band gap (eV)
$CoFe_2O_4$	36.44	498.90	6.48	1.61
$Co_{0.8}Cd_{0.2}Fe_2O_4$	26.65	299.18	2.97	1.72
$Co_{0.6}Cd_{0.4}Fe_2O_4$	23.35	249.84	3.08	1.73
$Co_{0.4}Cd_{0.6}Fe_2O_4$	16.94	60.76	0.70	1.72
$Co_{0.2}Cd_{0.8}Fe_2O_4$	6.83	39.2	0.14	1.72
$CdFe_2O_4$	2.59	49.97	60.87	1.64
$CoFe_2O_4/SiO_2$	28.50	686.88	6.14	1.67
$Co_{0.8}Cd_{0.2}Fe2O_4/SiO_2$	30.84	424.38	4.61	2.05
$Co_{0.6}Cd_{0.4}Fe_2O_4/SiO_2$	17.78	442.02	3.40	2.03
$Co_{0.4}Cd_{0.6}Fe_2O_4/SiO_2$	13.61	102.98	0.86	2.05
$Co_{0.2}Cd_{0.8}Fe_2O_4/SiO_2$	5.00	75.33	0.25	1.76
$CdFe_2O_4/SiO_2$	2.56	38.56	85.62	1.79

Where α_0 is a constant, $E = h\upsilon$ is the incident photon energy, α is the linear absorption coefficient. The power of the parenthesis (δ) is an exponent that depends on the type of the band transitions involved; e.g., $\delta = 1/2$ or $3/2$ for allowed direct inter band transitions and forbidden direct inter band transitions respectively, and $\delta = 2$ or 3 for allowed indirect inter band transitions and forbidden indirect inter band transitions respectively [33]. In this method, we need the thickness or concentration of the sample to be able to evaluate α using Beer-Lambert law; also this method employs the extrapolation of the linear portion of $(\alpha E)^{1/\delta}$ –E curve; this dependency on the linear extrapolation and thickness (or concentration) of the studied sample, can lead to some errors in the E_g-estimation, which as mentioned before, can affect the device optimization in applications.

In addition, in the Tauc method, the thing first required is to find the optimum value of optical transition index (δ). Recently, a new and more precise method (called as derivation of absorption spectrum fitting (DASF)) was proposed by Souri and Tahan [34] and was employed on the amorphous and nanocrystalline samples [35], and was found not to have any of the limitations of Tauc method, with no need of presuming δ. DASF method [34], is represented by the following relation (4):

$$\ln\left[\frac{A(\lambda)}{\lambda}\right] = \ln(D) + \delta \ln\left[\frac{1}{\lambda} - \frac{1}{\lambda_g}\right] \tag{4}$$

Where A (λ), λ, λ_g, and δ are absorption, wavelength, wavelength corresponding to the band gap, and optical transition index, respectively. Thus, by first derivation of Eq. 3 with respect to the ($1/\lambda$) the following, equation (5) is obtained:

$$\frac{d\{\ln[A(\lambda)/\lambda]\}}{d(1/\lambda)} = \frac{\delta}{\left(\frac{1}{\lambda} - \frac{1}{\lambda_g}\right)} \tag{5}$$

Referring to Eq. 4, there will be a discontinuity in the plot of $\frac{d\{\ln[A(\lambda)/\lambda]\}}{d(1/\lambda)}$ vs. ($1/\lambda$) at the absorption edge as $\frac{1}{\lambda} = \frac{1}{\lambda_g}$; so, by using the λ_g- value, E_g can be obtained precisely and directly from $E_g = 1239.83/\lambda_g$ in eV, in which there is no any presumption about the nature of transition (δ). Figs. 8-a and b show the collective UV-Visible spectra of bare and core-shell samples, respectively.

So, based on the above-mentioned viewpoints, the E_g values of the $Co_{1-x}Cd_xFe_2O_4/SiO_2$ nanocomposites with different Cd content were obtained through the use of DASF method, as the related DASF plots of before-mentioned bare and core-shell structures are shown in Figs. 9 and 10 for, respectively (the relevant discontinuity in DASF plots is depicted by a dashed-line as guide for the eye). The band gap values were estimated for the samples and the remarkable effects were observed by investigating their band gap results. As observed in Table 3, the estimated values are in the range of 1.61-2.05 eV, which are higher and lower than those estimated for pure $CdFe_2O_4$ and $CoFe_2O_4$ nanoparticles respectively.

In the literature, the E_g values are reported between 1.97 and 2.06 eV [33] for the $CdFe_2O_4$ nanoparticles and 1.2 and 1.92 eV [36] for the $CoFe_2O_4$ nanoparticles. Optical properties of nanocomposites are influenced by both the nature and quantity of nanoparticles in a matrix, along with the interaction at the interface between them. The band gap is affected by several factors such as particle size, presence of impurities, doping of substituent metal ion, and structural parameters [37]. Silica coated nanoparticles that demonstrate increasing tendency in the band gap values are as shown in Fig. 9. It may be due to the fact that silica is a wide band gap insulator with about 11eV in the bulk form [38].

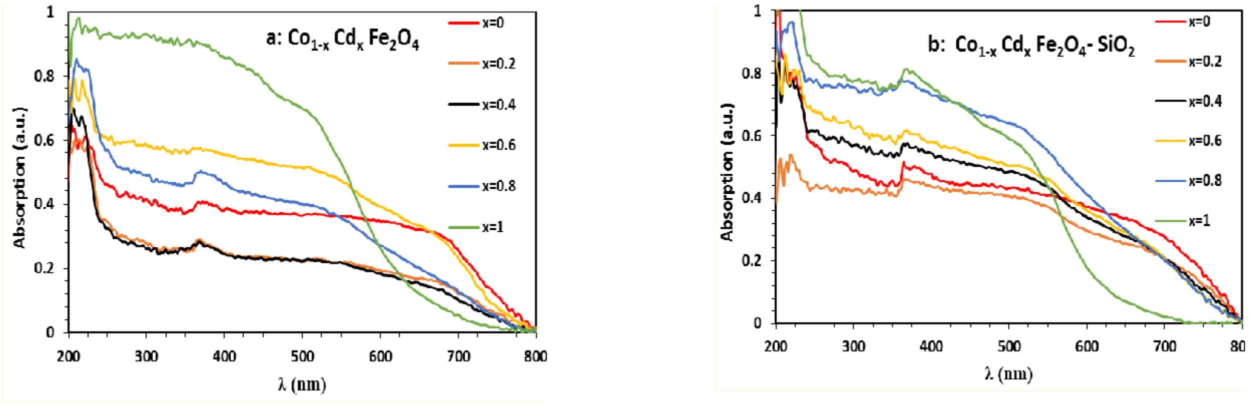

Fig. 8. UV-Vis Spectra of a: $CoFe_2O_4$ and b: Co Fe_2O_4-SiO_2.

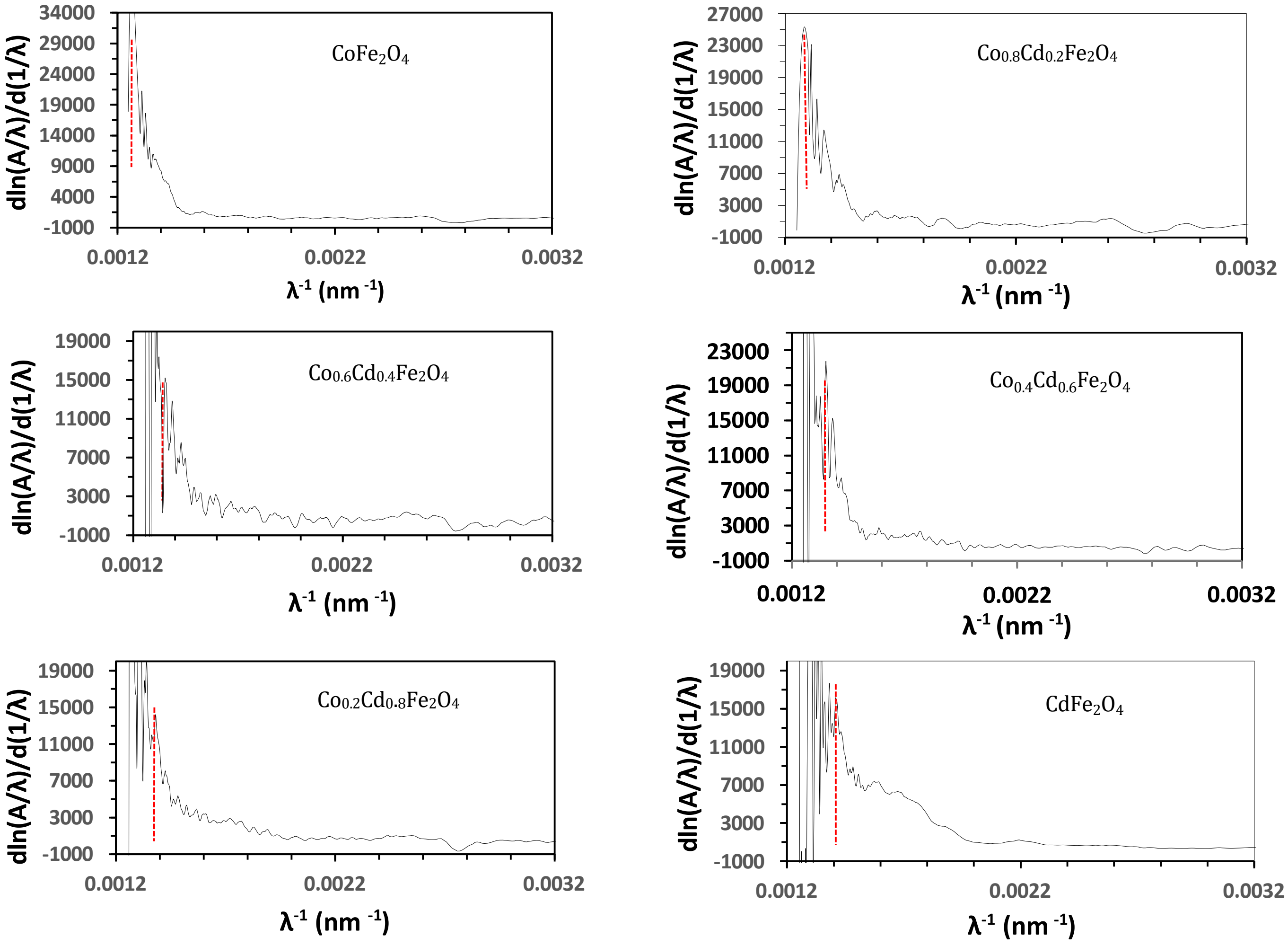

Fig. 9. DASF plot of d{ln(A/λ)}/ d(1/λ) versus (1/λ) for an uncoated $Co_{1-x}Cd_xFe_2O_4$ nanoparticles.

Another important parameter is the charge carrier optical transition nature, which can be evaluated based upon the DASF approach, employing Eq. 3; in this approach, the exact nature of optical transitions could be determined avoiding any presumption. Figs. 11-a and b show the typical curves of Ln(A/λ) vs Ln(1/ λ-1/ $λ_g$) for bare $CoFe_2O_4$ and $CoFe_2O_4$-SiO_2 core-shell structures, respectively. As illustrated in Fig. 11, δ (optical transition index) was determined from the slope of the linear part of Ln(A/λ)- Ln(1/ λ-1/ $λ_g$) plots. Results for the mentioned samples was around 1/2, which confirm the direct gap nature of the samples.

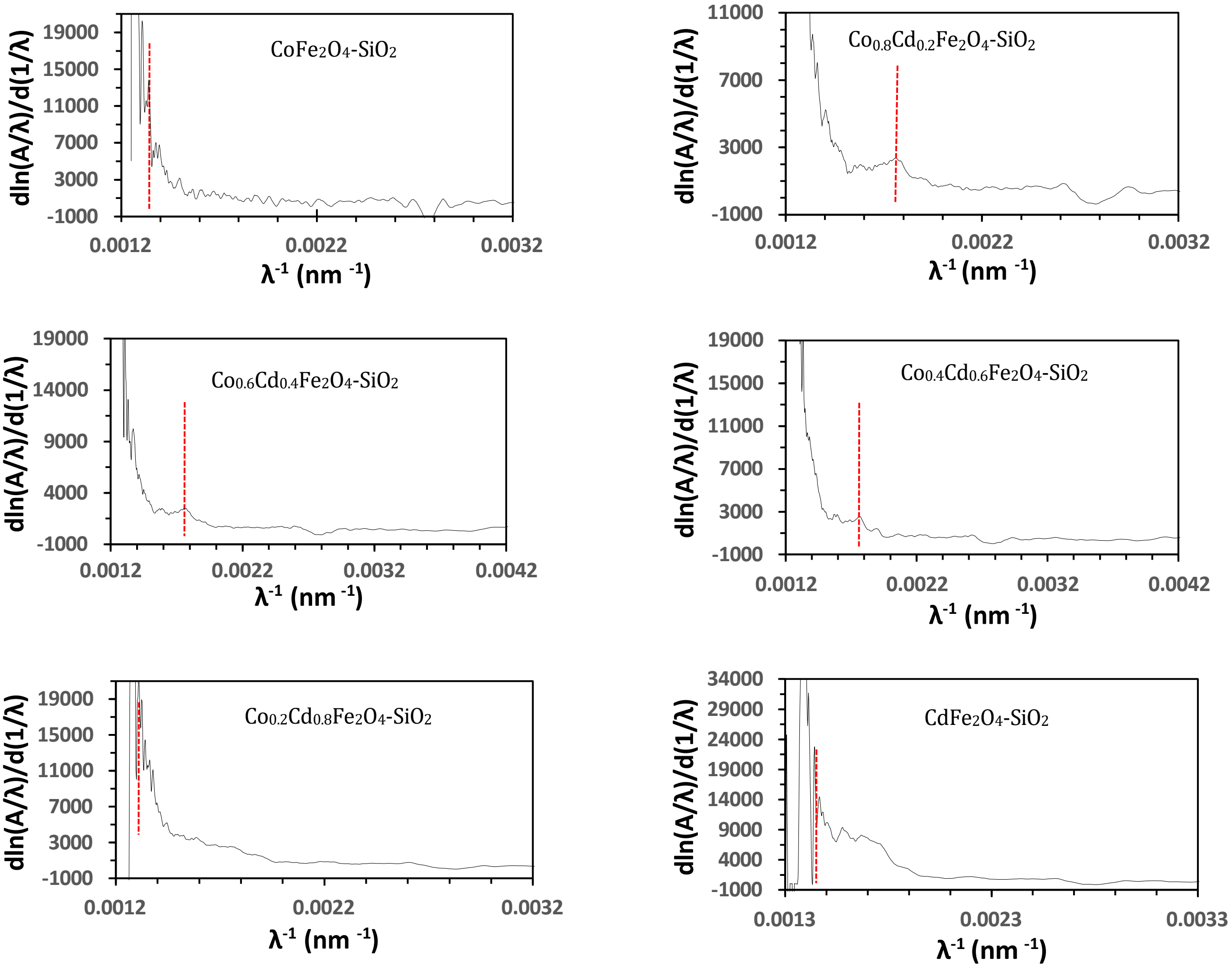

Fig. 10. DASF plot of d{ln(A/λ)}/ d(1/λ) versus (1/λ) for a coated $Co_{1-x}Cd_xFe_2O_4/SiO_2$ nanocomposites.

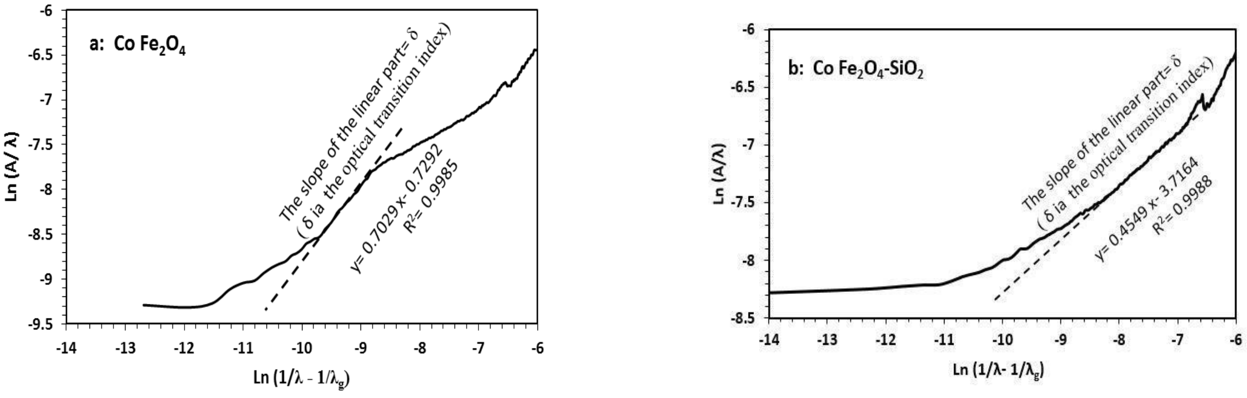

Fig. 11. Plots of Ln(A/λ)- Ln(1/ λ-1/ λg) for a: $CoFe_2O_4$ and b: Co Fe_2O_4-SiO_2.

5. Conclusion

$Co_{1-x}Cd_xFe_2O_4/SiO_2$ nanocomposites with core/ shell structure were prepared by coating of SiO_2 via the Stöber method on $Co_{1-x}Cd_xFe_2O_4$ nanoparticles and were synthesized by facile thermal treatment method. XRD patterns confirmed spinel ferrite structure for uncoated and SiO_2 coated nanocomposites. Increase in lattice parameters with increasing Cd^{2+} concentration was observed due to larger Cd^{2+} ionic radii. The FTIR spectra survey exposed the tetrahedral and the octahedral sites for uncoated and coated samples and confirmed the presence the bonds of Si–O–Si for coated samples. The

EDS analysis revealed the concentrations of Co, Cd, O, Fe, and Si included in the $Co_{0.4}Cd_{0.6}Fe_2O_4/SiO_2$ nanocomposites. TEM images disclosed the fine configuration and the thin size distribution of the nanoparticles as well as the uniform distribution of ferrite nanoparticles which dispersed in silica matrix. The changes in magnetic behaviors were attributed to the redistribution of cations between tetrahedral and octahedral sites upon replacement Cd^{2+} ions. The saturation magnetization and coercivity decreased with increasing Cd^{2+} concentration as a result of the lower anisotropy of Cd^{2+} ions in comparison with Co^{2+} ions and smaller magnetic moment per formula unit. Silica played a separation role among the nanoparticles to prevent the agglomeration and coarsening and therefore reducing the interparticle and magnetic dipolar interactions. The band gap energy (E_g) was estimated through the use of a precise DASF method, and so the influences of cadmium substitution and the SiO_2 coating on the band gap energy (E_g) were investigated. It was found that the addition of SiO_2 content to ferrite, leads to increase in optical band gap (E_g).

Acknowledgments

This work was supported by the Ministry of Science, Research and Technology, Malayer University of Iran.

References

[1] P. Vlazan, I. Miron, P. Sfirloaga, Cobalt ferrite substituted with Mn: Synthesis method, characterization and magnetic properties, Ceram. Int. 41 (2015) 3760-3765.

[2] E. Naderi, M. Naseri, H. Taimouri Rad, R. Zolfaghari Emameh, G. Farnoosh, A. Taheri1, In vivo and In vitro Biocompatibility Study of Fe3O4@ZnO and Fe3O4@SiO2 as Photosensitizer for Targeted Breast Cancer Drug Delivery, J. Sci. I. R. Iran. 31 (2020) 357 - 368.

[3] M. Naseri, Optical and magnetic properties of monophasic cadmium ferrite (CdFe2O4) nanostructure prepared by thermal treatment method, J. Magn. Magn. Mater. 392 (2015) 107-13.

[4] M. G. Naseri, E. B. Saion, H. A. Ahangar, A. H. Shaari, M. Hashim, Simple Synthesis and Characterization of Cobalt Ferrite Nanoparticles by a Thermal Treatment Method, J. Nanomater. 2010 (2010) 1-8.

[5] J. Z. Msomi, Structural and magnetic changes induced by high energy ball milling of $CdFe_2O_4$, J. Magn. Magn. Mater. 336 (2013) 61-65.

[6] M. G. Naseri, E. B. Saion, M. Hashim, A. H. Shaari, H. A. Ahangar, Synthesis and characterization of zinc ferrite nanoparticles by a thermal treatment method, Solid. State. Commun. 151 (2011) 1031-1035.

[7] R. G. Chaudhuri and S. Paria, Core/Shell nanoparticles: classes, properties, synthesis mechanisms, characterization, and applications, Chem. Rev.112 (2012) 2373-2433.

[8] M. E. Khosroshahi, L. Ghazanfari, Preparation and characterization of silica-coated iron-oxide bionanoparticles under N2 gas, Physica E Low Dimens. Syst. Nanostruct. 42 (2010) 1824-1829.

[9] L. Wang, K. G. Neoh, E. T. Kang, and B. Shuter, Multifunctional polyglycerol-grafted Fe_3O_4@SiO_2 nanoparticles for targeting ovarian cancer cells, Biomater. 32 (2011) 2166-73.

[10] M. Chireh, M. Naseri, Effect of calcination temperature on the physical properties of LiFe5O8 nanostructures, J. Adv. Pow. Tech. 30 (2019) 952-96022.

[11] B. J. Jankiewicz, D. Jamiola, J. Choma, M. Jaroniec, Silica–metal core–shell nanostructures, Adv. Colloid. Interface. Sci. 170 (2012) 28-47.

[12] J. M. Li, L. Wang, Z. H. Bai, J. Li, J. B. Lu, H. B. Li, Magnetic and Mössbauer spectroscopy studies of NiAl0.2Fe1.8O4/SiO2 nanocomposites synthesized by sol–gel method, J. Magn. Magn. Mater. 354 (2014) 190-194.

[13] D. Díaz, R. Bartolo, D.M. Delgadillo, F. Higueldo & J.C. Gomora, Contrasting Effects of Cd^{2+} and Co^{2+} on the Blocking/Unblocking of Human Cav3 Channels, J. Membr. Biol. 207 (2005) 91-105.

[14] R. Rani , P. Dhiman, S. K. Sharma &M. Singh, Structural and Magnetic Studies of Co0.6Zn0.4Fe2O4 nanoferrite synthesized by solution combustion method, Metal-Organic. Nano-Metal. Chem. 42 (2012) 360–363.

[15] M. G. Naseri, E. B. Saion, H. A. Ahangar, A. H. Shaari, Fabrication, characterization, and magnetic properties of copper ferrite nanoparticles prepared by a simple, thermal-treatment method, Mater. Res. Bull. 48 (2013) 1439-1446.

[16] H. SikChae, S. Deuk Kim, S. HaoPiao, H. J. Cho, Core-shell structured Fe3O4@SiO2 nanoparticles fabricated by sol–gel method and their magnetorheology, Colloid. Polym. Sci. 294 (2016) 647-655.

[17] A. Jamil, M. F. Afsar, F. Sher, M. A. Rafiq, Temperature and composition dependent density of states extracted using overlapping large polaron tunnelling model in MnxCo1−xFe2O4 (x=0.25, 0.5, 0.75) nanoparticles, Phys. B: Condens. Matter. 509 (2017) 76-83.

[18] C. Venkata Reddy, C. Byon, B. Narendra, D. Baskar, G. Srinivas, J. Shim, S.V. Prabhakar Vattikuti, Investigation of structural, thermal and magnetic properties of cadmium substituted cobalt ferrite nanoparticles, Superlattice Microst. 82 (2015) 165-173.

[19] L. Wang, M. Lu, Y. Liu, J. Li, M. Liu, H. Li, The structure, magnetic properties and cation distribution of Co1-xMgxFe2O4/SiO2 nanocomposites synthesized by sol–gel method, Ceram. Int. 41 (2015) 4176-4181.

[20] K. R. Awad, M. M. S. Wahsh, A. G. M. Othman, E Girgis, M. R. Mabroukand Fatma, A. Morsy, Effect of Mn2+ doping and SiO2 coating on magneto-optical properties of CoFe2O4, Smart Mater. Struct. 24 (2015) 115002-115006.

[21] M. G. Naseri, M. H. Majles Ara, E. B. Saion, A. H. Shaari, Superparamagnetic magnesium ferrite nanoparticles fabricated by a simple, thermal-treatment method, J. Magn. Magn. Mater. 350 (2014) 141-147.

[22] S. Kobayashi, T. Yamaminami, H. Sakakura, M. Takeda, T. Yamada, H. Sakuma, S. B. Trisnanto, S. Ota, Y. Takemura, Magnetization Characteristics of Oriented Single-Crystalline NiFe-Cu Nanocubes Precipitated in a Cu-Rich Matrix, Molecules. 25 (2020) 1-10.

[23] J. Massoudi, M. Smari, K. Nouric, E. Dhahri, K. Khirounid, S. Bertainae, L. Bessaisc, E. Kebir Hlil, Magnetic and

spectroscopic properties of Ni-Zn-Al ferrite spinel: from the nanoscale to microscale, RSC Adv. 10 (2020) 34556-34580.

[24] H. Sozeri, Z. Durmus, A. Baykal, Structural and magnetic properties of triethylene glycol stabilized ZnxCo1-xFe2O4 nanoparticles, Mater. Res. Bull. 47 (2012) 2442-2448.

[25] H. Ghorbani, M. Eshraghi , A. Sabouridodaran, Magnetic properties of $Co_{0.9}Cd_{0.1}Fe_{1.9}X_{0.1}O_4$ (X = Cr, Yb) nanoparticles prepared by hydrothermal method, Prog. physi. appl. mater. 1 (2021) 50-56.

[26] C. Choodamani, G.P. Nagabhushana, S. Ashoka, B. DarukaPrasad, B. Rudraswamy, G.T. Chandrappa, Structural and magnetic studies of Mg1−xZnxFe2O4 nanoparticles prepared by a solution combustion method, J. Alloys Compd. 578 (2013) 103-109.

[27] H. Hamad, M. Abd El-Latif, A. H. Kashyout, W. Sadikand, M. Feteha, Synthesis and characterization of core–shell–shell magnetic (CoFe2O4–SiO2–TiO2) nanocomposites and TiO2 nanoparticles for the evaluation of photocatalytic activity under UV and visible irradiation, New J Chem. 39 (2015) 3116-3128.

[28] M. Naseri, A. Kamalianfar, E. Naderi, A. Hashemi, The effect of Ag nanoparticles on physical and photocatalytic properties of ZnFe2O4/SiO2 nanocomposite, J. Mol. Struct. 1206 (2020) 127706.

[29] M. Atif, R. Sato Turtelli, R. Grössinger, M. Siddique, M. Nadeem, Effect of Mn substitution on the cation distribution and temperature dependence of magnetic anisotropy constant in Co1−xMnxFe2O4 (0.0≤x≤0.4) ferrites, Ceram. Int. 40 (2014) 471-478.

[30] K. Praveena, K. Sadhana, S. Ramana Murthy, Structural and magnetic properties of NiCuZn ferrite/SiO_2 nanocomposites, J. Magn. Magn. Mater. 323 (2011) 2122-2128.

[31] W. Pon-On, N. Charoenphandhu, I-Ming Tang, P. Jongwattanapisan, N. Krishnamra, R. Hoonsawat, Encapsulation of magnetic CoFe2O4 in SiO2 nanocomposites using hydroxyapatite as templates: A drug delivery system, Mater. Chem. Phys. 131 (2011) 485-494.

[32] C. Singh, A. Goyal, S. Bansal, S. Singhal, SiO2@MFe2O4 core-shell nanostructures: Efficient photocatalysts with excellent dispersion properties, Mater. Res. Bull. 85 (2017) 109-120.

[33] F. Miao, Z. Deng, X. Lv, G. Gu, S. Wan, X. Fang, Q. Zhang, Sh. Yin, Fundamental properties of CdFe2O4 semiconductor thin film, Solid. State. Commun. 150 (2010) 2036-2039.

[34] D. Souri, Z. E. Tahan, A new method for the determination of optical band gap and the nature of optical transitions in semiconductors, Appl. Phys. B: Lasers Opt. 119 (2015) 273-279

[35] D. Souri, A. R.Khezripour, M. Molaei, M.Karimipour; ZnSe and copper-doped ZnSe nanocrystals (NCs): optical transmittance and precise determination of energy band gap beside their exact optical transition type and Urbch energy; Current. Appl. Phys. 17 (2017) 41-46.

[36] P. A. Vinosha, L. AnselMely, J. E. Jeronsia, K. Raja, D. Queen SahayaTamilarsi, F. Alison christina, S. Krishnan, S. Jerome Das, Investigation of optical, electrical and magnetic properties of cobalt ferrite nanoparticles by naive co-precipitation technique, Optik. 127 (2016) 9917-9925.

[37] V. Etacheri, C. D. Valentin, J. Schneider, D. Bahnemann, C. P. J. Suresh, Visible-light activation of TiO2 photocatalysts: Advances in theory and experiments, J. Photochem. Photobiol. C. 25 (2015) 1-29.

[38] E. Vella, F. Messina, M. Cannas, R. Boscaino, Unraveling exciton dynamics in amorphous silicon dioxide: Interpretation of the optical features from 8 to 11 eV, Phys. Rev. B Condens. Matter. 83 (2011) 174201.